Hindawi
Geofluids
Volume 2023, Article ID 5089508, 16 pages
https://doi.org/10.1155/2023/5089508

Research Article

Numerical Simulations of Carbon Dioxide Storage Efficiency in Heterogeneous Reservoir Models

Evgeniy M. Myshakin,[1,2] **Foad Haeri**,[1,2] **Johnathan Moore**,[1] **Dustin Crandall**,[1] **and Angela L. Goodman**[1]

[1]*National Energy Technology Laboratory, 626 Cochran Mill Road, Pittsburgh, PA 15236, USA*
[2]*NETL Support Contractor, 626 Cochran Mill Road, Pittsburgh, PA 15236, USA*

Correspondence should be addressed to Evgeniy M. Myshakin; evgeniy.myshakin@netl.doe.gov

Received 21 December 2022; Revised 4 May 2023; Accepted 19 May 2023; Published 2 June 2023

Academic Editor: Daniele Cinti

The U.S. Department of Energy's National Energy Technology Laboratory (DOE-NETL) has been developing methods and tools (the online Carbon Dioxide Storage prospeCtive Resource Estimation Excel aNalysis (CO_2-SCREEN) tool) to estimate carbon dioxide (CO_2) storage potential in subsurface reservoirs. The CO_2 storage efficiency terms are input in the tool to calculate storage potential in targeted reservoirs. In this effort, two CO_2 storage efficiency terms were evaluated: volumetric displacement (E_V) and microscopic displacement (E_d). The first term deals with efficiency of CO_2 propagation into an accessible reservoir volume, while the second term evaluates effectiveness of native fluid displacement with CO_2. The interpreted well logs and core sample measurements were applied to create the heterogeneous reservoir models including geostatistical realizations of porosity and intrinsic permeability fields. Supercritical CO_2 was injected over the course of 30 years into brine-saturated reservoir models for clastics, limestone, and dolomite lithologies and deltaic fluvial, aeolian, shallow marine, and reef depositional environments by means of varying reservoir parameters and injection scenarios. The reservoir models providing vertically heterogeneous petrophysical properties and designated as "layered reservoir models" (with homogeneous parameters along each layer of the model) were not determined to be a transition between the homogeneous and heterogeneous models in respect to storage efficiency. Another finding shows that high-efficiency factors do not necessarily mean increased CO_2 storage; they rather indicate that the available volume and pore space are more fully utilized. The CO_2 storage efficiency factors were evaluated dynamically at the select time points using P_{10}-P_{50}-P_{90} percentiles. The results of this study show that the P_{10}-P_{90} distribution for volumetric efficiency is wider when compared to the microscopic efficiency. It was found that where dominant buoyancy forces drive the plume to the top of a target formation, the volumetric efficiency is low. Tighter sandstone and carbonate formations show prevalence of capillary forces and better utilization of reservoir volume.

1. Introduction

Subsurface storage of CO_2 is gaining interest as a means for mitigating greenhouse gas emissions. There is a need for development of methods that estimate how much CO_2 can be stored in the subsurface to be widely available and easily accessible. Recently, a standard guide for estimating storage of CO_2 in the subsurface with consistent terminology was developed by the Society of Petroleum Engineers (SPE) and the American Association of Petroleum Geologists (AAPG) called the Storage Resources Management System (SRMS) [1]. This system focuses on developing a framework for large-scale commercial storage of CO_2 in the subsurface where a project is clearly defined with active injection wells and the amount of storage space available is quantified. There are three storage classifications under the SRMS: storage capacity, contingent storage resources, and prospective storage resources. Capacity quantifies storable quantities for developed projects actively injecting CO_2, while both contingent and prospective storage resources cover projects that are not proven but include various degrees of regional assessments. The U.S. Department of Energy National Energy

Technology Laboratory (DOE-NETL) has worked to develop storage methods at the contingent and prospective storage levels for saline formations, unmineable coal seams, depleted unconventional shale formations, and residual oil zones [2–5]. An online version of these methods is available as the CO_2 Storage prospeCtive Resource Estimation Excel aNalysis (CO_2-SCREEN) tool [3]. These methods and tools have been used worldwide to estimate contingent storage and prospective storage and incorporated into best practice field manuals compiled from CO_2 injection tests at various pilot-scale sites [6–10]. The introduction of CO_2 storage efficiency factors utilized in the CO_2-SCREEN tool is provided below.

The U.S. DOE is considering geologic carbon storage as a means for reducing anthropogenic emission of CO_2 that contributes to climate change and formed a nationwide network of regional partnerships to help determine the best approaches for capturing and permanently storing CO_2 [10]. The U.S. DOE Carbon Storage Program also developed a CO_2 storage method in conjunction with the Regional Carbon Sequestration Partnerships (RCSP) for the estimation of volumetric CO_2 storage in deep saline formations, oil and gas reservoir, and unmineable coal seams in the U.S. and portions of Canada [6–9]. The RCSP were government/industry efforts tasked with determining the most suitable technologies, regulations, and infrastructure needs for carbon capture, storage, and sequestration in different areas of the country [10]. Saline aquifers show high potential in terms of storage potential and safety as evidenced by development phase field projects for CO_2 storage [10].

As reported in Ref. [11], the U.S. DOE-NETL methodology introduces a volumetric method to estimate prospective mass CO_2 storage resource (G) using

$$G = A^d h^s \phi^s \rho^s E_{\text{saline}}{}^s, \tag{1}$$

where A^d, h^s, ϕ^s, and ρ^s are the areal size of the formation, the thickness of the formation, porosity, and CO_2 density (estimated at average pressure and temperature of the storage formation), respectively. Superscripts d and s indicate that a corresponding parameter is estimated deterministically and stochastically (the superscripts are further omitted for clarity).

The storage efficiency (E_{saline}) term reduces the estimation of stored CO_2 mass at a specific site to accommodate the complexities of the fundamental processes associated with production, injection, and storage within saline aquifers.

$$E_{\text{saline}} = E_A E_h E_\phi E_V E_d, \tag{2}$$

$$E_{\text{saline}} = \frac{1}{\left(1 + e^{(-E_A)}\right)} * \frac{1}{\left(1 + e^{(-E_h)}\right)} * \frac{1}{\left(1 + e^{(-E_\phi)}\right)} * \frac{1}{\left(1 + e^{(-E_V)}\right)} * \frac{1}{\left(1 + e^{(-E_d)}\right)}, \tag{3}$$

where E_A, E_h, and E_ϕ are the fraction of the geologic area, thickness, and porosity accessible for CO_2 storage, respectively. Since the individual efficiency terms in Equation (2) are determined stochastically, Equation (2) is required to be written in log odds notation and expanded to Equation (3) (as described in Ref. [9]) to determine storage efficiency (E_{saline}) using Monte Carlo sampling.

E_V, the volumetric displacement efficiency, represents the fraction of reservoir volume accessed by CO_2 plume. It is calculated as the ratio of CO_2 injected to the pore volume of the reservoir accessed by the CO_2 plume.

$$E_V = \frac{V_i}{Ah\phi\left(1 - S_{w_{\text{irr}}}\right)} = \frac{Q_i t}{Ah\phi\rho\left(1 - S_{w_{\text{irr}}}\right)}, \tag{4}$$

where V_i is the volume of injected CO_2; A, h, and ϕ are the area, thickness, and porosity of the accessed volume, respectively; and $S_{w_{\text{irr}}}$ is the irreducible water saturation. The volume of the injected CO_2 can also be expressed through mass flow rate (Q_i), injection duration (t), and averaged CO_2 density (ρ) at *in situ* conditions (Equation (4)). To determine the area, A, the minimum-area-circle approach is used as depicted in Figure S1 (Supplemental Materials). The accessible volume is the multiplication of the area and thickness of the formation.

E_d, the microscopic displacement efficiency, is the fraction of water displaced by CO_2, which is calculated at the plume level by the average water saturation ($S_{w_{\text{ave}}}$) as shown in Equation (4) [12].

$$E_d = 1 - S_{w_{\text{ave}}} = S_{\text{CO}_{2\text{ave}}}, \tag{5}$$

where $S_{\text{CO}_{2\text{ave}}}$ is the average CO_2 saturation within the CO_2 plume. It is assumed that CO_2 would not be able to occupy all effective porosity defined by $(1 - S_{w_{\text{irr}}})$ [12].

The volumetric and microscopic displacement efficiencies are dynamic terms in Equation (2) and Equation (3) since their values are time-dependent and change with the CO_2 plume propagating through a target formation. As injection progresses with time, plume shape changes and, therefore, E_V changes. In addition, E_d changes as average saturation values change due to buoyancy forces, capillary trapping, and other processes. The time dependency of storage efficiencies emphasizes the importance of the heterogeneous representation of porosity and intrinsic permeability in reservoir models mimicking actual pore network in a saline aquifer and coupled permeability controlling mobile phase flow.

Shao et al. [13] performed simulations on various stochastic model realizations under different conditions and showed that nested geological heterogeneity is a major player in controlling plume propagation. Rasheed et al. [14] found that an aquifer with a porosity higher than 20% and a low to medium level of heterogeneity is more suitable for CO_2 storage. Stochastically generated and spatially correlated permeability distributions have shown that heterogeneous permeability significantly affects both the accumulation and distribution of CO_2 [15–17]. Heterogeneity also promotes the local capillary trapping that may deviate the path of rising CO_2 [18, 19]. Both experimental and numerical studies have identified the great impact of

heterogeneous capillary trapping on the performance of CO_2 storage [20, 21].

Several studies have explored CO_2 storage in saline formations using numerical simulation [22]. Storage potential and efficiency factors have been investigated by developing heterogeneous models and performing sensitivity analysis using geologic (e.g., ratio of net to gross thickness, ratio of net to total area, and ratio of effective to total porosity), macroscopic (e.g., gravity), and microscopic (e.g., saturation) terms [23]. To estimate storage efficiency for specific lithologies and depositional environments, heterogeneous geocellular models and geological architecture common to each of the environments had to be developed [24–26]. However, prior storage efficiency values were mostly based on limited geologically nonspecific relative permeability data.

Recently, CO_2 storage capacity in deep saline aquifers and residual oil zones (ROZs) was investigated using machine learning algorithms [27, 28]. The developed smart tools could be used to provide fast and accurate storage efficiency for aquifers that have similar parameters falling within the range of the database [27]. The proposed artificial neural network models can predict the CO_2-enhanced oil recovery (EOR) and storage performance with high accuracy in ROZs [28].

In our recent work, storage efficiency parameters were estimated based on homogeneous reservoirs [29]. Homogeneous CO_2 storage efficiency values for supercritical CO_2 injection into brine-saturated reservoirs for clastics, limestone, dolomite lithologies and marginal marine, strand plain, deltaic complex fluvial, aeolian, shallow marine, and reef depositional environments were determined for 30 years of injection [29]. In this work, we add complexity to the storage efficiency factors by incorporating heterogeneity into the reservoir models. The numerical simulations of fluid dynamic models to estimate volumetric displacement (E_V) and microscopic displacement (E_d) efficiency factors for saline formations were performed using the TOUGH3 code [30]. In this effort, heterogeneity was accounted for in the reservoir models designed for CO_2 injection using downhole well log information retrieved at pilot sites of different lithologies and depositional environments. The models are developed using the corresponding experimental relative permeability data available in the CO_2-Brine Relative permeability Accessible (CO_2BRA) database [31]. The heterogeneous storage efficiency values are also available in DOE-NETL's CO_2-SCREEN tool v4.1 [3].

2. Methodology

The workflow of the manuscript includes creating heterogeneous reservoir models that represent five combinations of lithology and depositional environment. Next, simulation cases are run with varying pressure, temperature, permeability anisotropy, injection rate, reservoir thickness, porosity, and permeability distributions. Then, the results of CO_2 injection over 30 years are processed to calculate time-dependent storage efficiency terms using Equations (4) and (5). The computed efficiency factors are then analyzed and compared with factors estimated using homogeneous reservoirs. A summary table listing the storage efficiency factors as P_{10}-P_{50}-P_{90} percentiles is provided at the end of the manuscript.

2.1. DOE Carbon Storage Partnership Sites Used as Proxy for Heterogeneous Reservoir Models. Five saline reservoir models and five depositional environments were considered in this study based on the data collected by the RCSP. The heterogeneous reservoir models were based on the corresponding sections of saline aquifers showing the best quality in terms of total porosity and intrinsic permeability for continuous CO_2 injection. Below is the list of the formation/depositional environments utilized for making the models and their brief descriptions. A suite of wireline logs was collected at each site and interpreted with core sample measurements to provide total porosity and intrinsic permeability distributions within the reservoir thickness. Supplemental material contains derived porosity and permeability logs used to create the heterogeneous reservoir models (Figures S2, S5, S7, S10, and S13).

(1) *Lower Mt. Simon Sandstone/Shallow Marine* (3,320-3,507 ft. (1012-1069 m) true vertical depth below ground surface (TVDbgs) (187 ft. (57 m) total) at Duke Energy #1 Well (East Bent Field, Boone County, Kentucky)). The field project conducted at the Duke Energy East Bend Generating Station in Boone County, Kentucky, was carried out within the Midwest Regional Carbon Sequestration Partnership. The Mt. Simon Sandstone represents the target injection reservoir at the East Bend site. Based on the core sample analysis, the reservoir is sand-dominated consisting of a fine- to coarse-grained quartz in a lower shoreface (shallow marine) depositional environment [32]

(2) *Cranfield Sandstone/Fluvial* (10,430-10,505 ft. (3179-3202m) measured depth (MD) (75 ft. (23 m)) and 10,598-10,630 ft. (3230–3240 m) MD (32 ft. (10 m)) at CFU 31F#1 Injection Well (Cranfield Unit, Lincoln County, Mississippi)). This field project is being conducted at the Cranfield Site, Franklin, Mississippi, within the framework of Southeast Regional Carbon Utilization and Storage Partnership. The target reservoir in the Tuscaloosa Formation at Cranfield Site represents fluvial sandstone containing high amounts of volcanoclastic grains [33]. The volcanoclastic grains were dissolved during early diagenesis and served as a source for quartz cements. Chlorite cement prevented precipitation of additional cement and preserved high porosity as deep as 1.86 miles (~3 kilometers)

(3) *Broom Creek Sandstone/Aeolian* (6,280-6,457 MD ft. (1914-1968 m) (177 ft. (54 m)) at Flemmer Well #1 (Wildcat Field, North Dakota)). In spring 2017, the Energy & Environmental Research Center initiated an effort to determine the feasibility of developing a commercial-scale CO_2 geologic storage complex able to store more than 50 million tons (Mt) of CO_2 in

Table 1: Formation and CO_2BRA sample names corresponding to similar lithology and depositional environments and CO_2BRA sample porosity, permeability (mD), and parameters* of relative permeability curves.

N	Formation name	Lithology	Depositional environment	CO_2BRA sample name	Sample porosity	Sample perm. (mD)	S_{wir}	k_{rw}^{max}	S_{CO2ir}	k_{rCO2}^{max}
1	Lower Mt. Simon	Sandstone	Marginal marine	Bandera Brown A	0.164	124	0.566	1.00	0.00	0.320
2	Cranfield	Sandstone	Deltaic complex fluvial	Castlegate	0.252	865	0.705	1.00	0.00	0.185
3	Broom Creek	Sandstone	Aeolian	Navajo	0.156	41	0.497	1.00	0.00	0.271
4	Middle Duperow	Carbonate, limestone	Shallow marine	Edwards Yellow	0.192	25	0.460	1.00	0.01	0.102
5	Bass Island	Carbonate, dolomite	Shallow marine/reef	Silurian	0.129	327	0.453	1.00	0.10	0.032

*Where S_{wir} and S_{CO2ir} are the residual water and $scCO_2$ saturations and k_{rw}^{max} and k_{rCO2}^{max} are the maximum brine and $scCO_2$ relative permeability values.

central North Dakota safely, permanently, and economically. The geologic characterization well was drilled in the Broom Creek Formation, which represents a quartz-dominated sandstone, and sidewall core samples were retrieved from the well [34]. The depositional environment of the Broom Creek Formation is aeolian [35]

(4) *Middle Duperow Carbonate/Reef* (3,280-3,450 MD ft. (1000-1052 m) (170 ft. (52 m)) at Danielson 33-17 Well (Kevin Dome formations, Kevin Sunburst Field, Toole County, Montana)). The Big Sky Carbon Sequestration Partnership (BSCSP, now the part of Carbon Utilization and Storage Partnership of the Western United States) was supported through a cooperative agreement with DOE. BSCSP's goal was to demonstrate that the Kevin Dome is a safe and viable location for the long-term storage of CO_2. The Middle Duperow Carbonate (mixed limestone and dolostone) formation was selected as a target formation, and the Danielson 33-17 Well was drilled through the formation [36]

(5) *Bass Islands Dolomite/Shallow Marine* (3,440-3,515 MD ft. (1048-1071 m) (75 ft. (23 m)) at St. Charlton 4-30 Well (St. Charlton, Otsego County, Michigan)). As part of the Midwest Regional Carbon Sequestration Partnership Phase II research program, the St. Charlton 4-30 Well was drilled and logged in northeastern Otsego County, Michigan. The Bass Islands Group (BILD) is carbonate, and evaporitic sedimentary rocks were produced by the diagenetic alteration of Late Silurian shallow water in Michigan and the eastern Great Lakes region. The BILD, deposited in a shallow marine environment, is dominantly dolomite with locally high porosity and permeability due to grainstone and collapsed karst textures. Porosity ranges from 2% to 38% with an average of 13%. Permeability ranges from 0 mD to 684 mD with an average of 23 mD. The Core Energy St. Charlton #4-30 well drilled through at least 188 ft. (57 m) of BILD and collected 78 ft. (24 m) of core from the uppermost part along with 42 ft. (13 m) of the overlying Bois Blanc Formation [37]

2.2. CO_2BRA Database of Relative Permeability Data for Select Lithologies and Deposition Environments. Besides heterogeneity of the petrophysical properties in a target formation, another strong factor influencing the efficiency terms is relative permeability (k_r) controlling multiphase flow in pore space. The impact of different k_r relationships and their parameters is critical to accurately predict the propagation supercritical CO_2 ($scCO_2$) and saturation distribution in a reservoir [38, 39]. In this study, CO_2BRA, a freely available database containing experimental data for rock types of different depositional environments [31, 40], was utilized to correlate lithology and depositional environment of the select heterogeneous reservoir models with k_r experimental data measured for corresponding core samples. The k_r data for the corresponding lithology/deposition were made available in the TOUGH3 code [30] used to conduct simulations. Details of the CO_2BRA database implementation into the code and selection of experimental k_r curves for a lithology/deposition environment of interest can be found elsewhere [29].

Table 1 lists the five target formations and their dominant deposition environments, described in the previous section, against relevant CO_2BRA sample names of the same lithology and deposition. The table also collects porosity, permeability, and parameters of residual saturations and maximum k_r values derived from the unsteady-state experiment of CO_2 injection into the brine-saturated core samples [40]. Noticeably, there are low endpoint k_r values of CO_2 (<0.3) and high residual brine saturations (>0.4) for the k_r curves that were typical for the unsteady-state method of $scCO_2$ injection [41, 42]. The method relies on the injection of $scCO_2$ to displace brine in a fully saturated sample and never truly settles on a steady-state condition due to the incremental displacements of the primary fluid [43, 44]. The low endpoint numbers for $scCO_2$ and high residual saturation values for brine are attributed to capillary end effects, sample heterogeneity, and low mobility ratio by Jeong et al. [45].

Supplemental material contains descriptions of sidewall core samples (where available) extracted at the geological wells and the CO_2BRA samples corresponding to similar lithology and depositional environment (Figures S3, S4, S6, S8, S9, S11, S12, S14, and S15 and Tables S1-S2). The images of the samples are accompanied with general

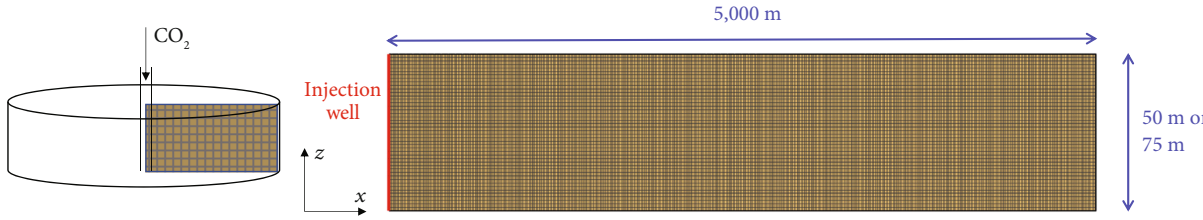

Figure 1: Utilization of the cylindrical 3D domain to generate a 2D reservoir model.

geological descriptions and, at certain cases, information about grain size indices and mineralogy.

2.3. Reservoir Model Preparation. The heterogeneous reservoir models were approximated using a vertical cylindrical model with a wellbore placed along its axis (Figure 1). Taking advantage of the cylindrical symmetry, 2D axisymmetric models were created using 5,000 m as a reservoir radius in the lateral direction and a wellbore placed on the left boundary of a 2D model. The meshes were created using quadrilateral grid blocks with CO_2 entering through a wellbore perforated along the length of reservoir thickness. The meshes consist of 35 uniformly spaced grid blocks in the lateral direction (X-coordinate) with 42 and 62 cells in the vertical direction (Z-coordinate) for 50 and 75 m reservoir thickness, respectively. That produces 35×42 and 32×62 mesh sizes. No-flow boundaries at the top and the bottom and open-flow boundaries at the lateral extent of the reservoir are assumed. The mesh size sensitivity analysis was conducted to confirm that finer mesh sizes provide similar numerical results. The reservoir models were created flat focusing on the geologic heterogeneity of the rocks.

To populate the mesh with porosity and permeability data, the well log information depicted in Figures S2, S5, S7, S10, and S13 and core measurement correlations (Supplemental Materials) were used. Two types of heterogeneity were introduced into the reservoir models: (1) *layered*. Porosity and permeability values were varied with depth following the mesh discretization in the vertical direction. To do so, the corresponding values were upscaled (red lines in the above-mentioned figures in Supplemental Materials) to fit layers of the meshes. In the lateral direction, the properties were assigned uniformly assuming they are laterally homogeneous. This model implies ideal geological control of the properties in the horizontal directions. (2) *Heterogeneous*. For those models, the density porosity logs across the reservoir thickness were utilized to estimate empirical variograms in the vertical direction. Since only one well log was adopted for each formation, to quantify spatial correlation in the lateral direction, the anisotropy factors were applied following the guidance from Gorecki et al. [23] for horizontal variogram ranges or information about geologic control of bedding planes at nearby wells if available (like for Danielson and Wallewein wells drilled into the Middle Duperow formation) [46]. Since the reservoir models utilize a 2D approximation, no azimuthal control for model variogram was used. That implies the same geospatial property correlation in the horizontal direction. Using the model variogram as weighting functions, ordinary kriging along with Sequential Gaussian Simulation was performed using the normal score-transformed porosity as the input data on a rectangular reservoir grid. The output from the stochastic simulation, which is a normal score porosity, was transformed back to actual porosity values. A geostatistical software, WinGSLib v.2015 [47], was used to calculate porosity distributions for each heterogeneous reservoir model. To generate coupled intrinsic permeability data, the correlation derived from permeability logs, or core measurements, was used to develop permeability values. Up to nine realizations of porosity and coupled permeability distributions were generated for use in simulations to account for uncertainty in property distributions. Figure 2 shows the layered and heterogeneous representation of the sandstone/fluvial reservoir models generated using the Cranfield Sandstone formation as a proxy.

The initial pressure and temperature conditions were selected based on data from Gas Information System (GASIS) [48], which is a public database containing approximately 20,000 oil and gas reservoir records. The initial P-T values correspond to CO_2 in supercritical condition. CO_2 injection was executed for 30 years using an open interval across the entire reservoir thickness. Table 2 collects pertinent reservoir model parameters and injection scenarios. The simulation cases designed to estimate statistical distributions of the CO_2 storage efficiency terms are considered in the next section.

2.4. Simulation Cases. For each combination of lithologies and depositional environments listed in Table 1, simulation cases were designed by varying five parameters for sensitivity analysis, as shown in Table 3.

They included pressure, temperature, permeability anisotropy (i.e., the ratio of vertical permeability to horizontal permeability, k_v/k_h), reservoir thickness, and injection rate. A min/max value was selected for each parameter. The min/max pressure was coupled with min/max temperature representing shallow/deep formations, respectively. The minimum pressure and temperature were selected in such a way to assure the existence of $scCO_2$. The min/max for permeability anisotropy was set at 0.1 and 0.5 [52, 53]. The min/max injection rates were selected in such a way to be consistent with field data [32–37] and the maximum pressure buildup around the wellbore and formation fracture pressure [29]. The thickness variability was based on consideration of typical perforation intervals

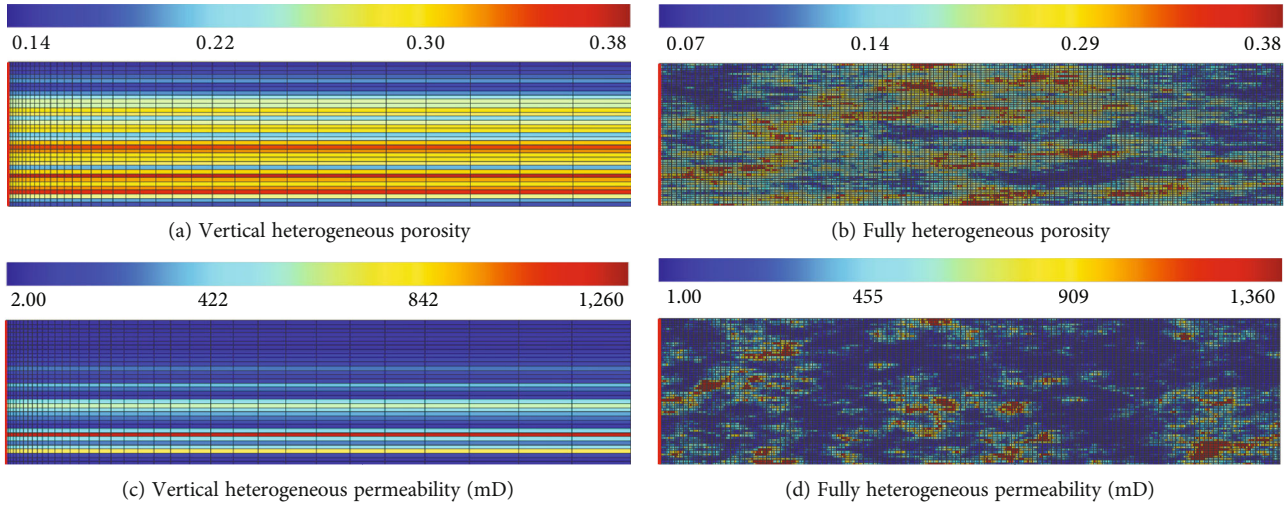

(a) Vertical heterogeneous porosity

(b) Fully heterogeneous porosity

(c) Vertical heterogeneous permeability (mD)

(d) Fully heterogeneous permeability (mD)

Figure 2: Layered and heterogeneous porosity (a, b) and layered and heterogeneous permeability (c, d) distributions of the sandstone/fluvial reservoir.

Table 2: Model parameters and injection scenarios.

Mesh size and model dimensions	
Length	5,000 m
Thickness	55 and 75 m
Mesh size	35×42 and 35×62
Number of elements	1,470 and 2,170
Rock properties	
Porosity	Heterogeneous
Permeability	Heterogeneous
Number of geostatistical realizations	9
Relative permeability	CO_2BRA database
Capillary pressure	Lithology-sensitive*
Initial conditions	
Initial pressure	GASIS database
Pressure gradient	10.14 kPa/m
Initial temperature	GASIS database
Temperature gradient	0.02°C/m
Brine concentration	8 wt.%
Pore compressibility	4.5^{-10} Pa^{-1}
Injection scenarios	
Injection rate	400 and 800 tons/day
Injection period	30 years
Perforation	Reservoir thickness

*For sandstone reservoir models, the Brooks-Corey capillary pressure function was used using the parameters from Refs. [49, 50], and for limestone and dolomite reservoir models, the van Genuchten capillary pressure function was utilized using the parameters from Ref. [51]. Leverett scaling of capillary pressure was invoked since heterogeneous porosity and permeability fields were used.

positioned against reservoir sections with largest permeability in the target formations [34].

In this study, the numerical simulations were carried out using the ECO2M module of TOUGH3 [30] designed for simulations of CO_2 storage in saline aquifers. The module represents a comprehensive description of thermodynamic properties of a H_2O-NaCl-CO_2 mixture [54] within broad ranges of pressure, temperature, and salt concentrations. The module accounts for phase changes that can arise during CO_2 injection involving gaseous, liquid, and supercritical phases of CO_2 together with brine and has improved convergence during the appearance and disappearance of a nonaqueous phase. PetraSim [55] was used to postprocess the results of the simulations.

3. Results and Discussion

Table 3 lists 16 total cases created using various injection scenarios and reservoir parameters, which together with nine geostatistical realizations of porosity and coupled permeability distributions for each case provide 144 simulations carried out for each reservoir model type: layered and heterogeneous models. In total, 288 simulation runs were conducted. The results of the simulations were postprocessed following the approach described in Section 2 to calculate CO_2 efficiency terms and corresponding percentile values (Equations (4) and (5)). Figure 3 compares volumetric displacement efficiency (E_V) and microscopic displacement efficiency (E_d) computed using layered and heterogeneous reservoir models with homogeneous values calculated in the previous study [29] for select lithology/depositional environment. The efficiency terms are represented as horizontal bars (probability distribution ranges) where the minimum and maximum values correspond to P_{10} and P_{90} values (10^{th} and 90^{th} percentile), respectively. The table also contains minimum and maximum porosity and permeability values extracted from the GASIS database [48] for homogeneous models and average porosity/permeability values evaluated using layered and heterogeneous (one realization) reservoir models.

The analysis of Figure 3 indicates that introducing geologic heterogeneity into petrophysical properties strongly

Table 3: Example of parameters used for sensitivity analysis (Lower Mt. Simon).

Modeling cases							
Model no.	Temperature (°C)	Pressure (MPa)	K_v/K_h	Rate (tons/day)	Thickness (m)	Porosity	Permeability
1	32.2	9.65	0.5	400	55	Heterogeneous	Heterogeneous
2	32.2	9.65	0.5	800	55		
3	32.2	9.65	0.1	400	55		
4	32.2	9.65	0.1	800	55		
5	87.8	27.6	0.5	400	55		
6	87.8	27.6	0.5	800	55		
7	87.8	27.6	0.1	400	55		
8	87.8	27.6	0.1	800	55		
9	32.2	9.65	0.5	400	75		
10	32.2	9.65	0.5	800	75		
11	32.2	9.65	0.1	400	75		
12	32.2	9.65	0.1	800	75		
13	87.8	27.6	0.5	400	75		
14	87.8	27.6	0.5	800	75		
15	87.8	27.6	0.1	400	75		
16	87.8	27.6	0.1	800	75		

influences flow characteristics determining the plume size and shape. This translates into broad variations of the volumetric efficiency that range from 11.5% in sandstone/aeolian to 90.5% in carbonate/shallow marine depositional environments. In some cases, probability distribution ranges of volumetric efficiency become narrower by adding heterogeneity (e.g., sandstone aeolian), and in others, ranges become wider (e.g., carbonate reef limestone). Given that the volumetric efficiency is based on a CO_2 plume shape and maximum propagation of CO_2 into pore space of a saline aquifer, it is expected that the volumetric efficiency is sensitive to porosity and permeability distributions in a reservoir. The results indicate that there is no trend in probability range changes moving from homogeneous to layered and then to heterogeneous models. We also concluded that layered models utilizing idealistic property distribution in the lateral direction cannot be considered as "transition" models from homo- to heterogeneous models in terms of volumetric efficiency evaluation. Since layered models use only vertical variability in porosity and permeability, locations of layers with high values of porosity and permeability in the horizontal direction (Figures S2, S5, S7, S10, and S13) facilitate plume extension into those layers and determine an efficiency value.

Microscopic efficiency ranges are generally less impacted and demonstrate narrow ranges compared to the distribution ranges of the volumetric efficiency. Only the carbonate/reef data show wide distribution ranges for both layered and heterogeneous models. For that combination of lithology and deposition, large shifts are observed in both microscopic and volumetric efficiency ranges, moving from homogeneous to layered and then to heterogeneous models. These variations of CO_2 plume shape and storage efficiencies are further explained in Figure 4. The presence of high permeable layers (Figure S13) in the middle of the layered model (Figure 4(b)) allows for CO_2 to channel through the formation, resulting in a different plume shape compared to the homogeneous or heterogeneous models (Figures 4(a) and 4(c)). As a result, volumetric efficiency is reduced because of the extended plume shape for the layered model. Reduction of microscopic efficiency of the layered model is associated with diminishing of CO_2 saturation in the areas behind the advancing CO_2 front. Such behavior indicates dominance of capillary trapping over transverse buoyancy crossflow and is typical for layered systems of contrasting porosity/permeability [56]. The heterogeneous model provides a larger E_V value when compared to the homogeneous model (Figures 4(a) and 4(c)). In the heterogeneous case, the efficiency term is calculated based on the minimum-area-circle approach (Figure S1) and near vertical plume interface which results in more effective reservoir volume utilization.

Thus, the balance between viscous, capillary, and buoyancy forces affects the efficiency terms. A dimensional analysis has been widely used to characterize multiphase fluid flow in porous media to quantify the ratio of a certain force over another one [57–60]. The residually trapped nonwetting phase is directly affected by a tradeoff between viscous, capillary, and buoyancy forces and was shown to be correlated with dimensionless number magnitude, like capillary and bond numbers [61–65]. To analyze dominant forces acting during CO_2 flow in porous media of the reservoir, the dimensionless bond (B_o) number was engaged which assesses the ratio of gravitational (negative to buoyancy) and capillary forces (Equation (6)) from Shook et al. [66], Kuo and Benson [67], Trevisan et al. [68], and Ben [69].

$$B_o = \frac{\Delta\rho g k_V}{\sigma \cos\theta}, \tag{6}$$

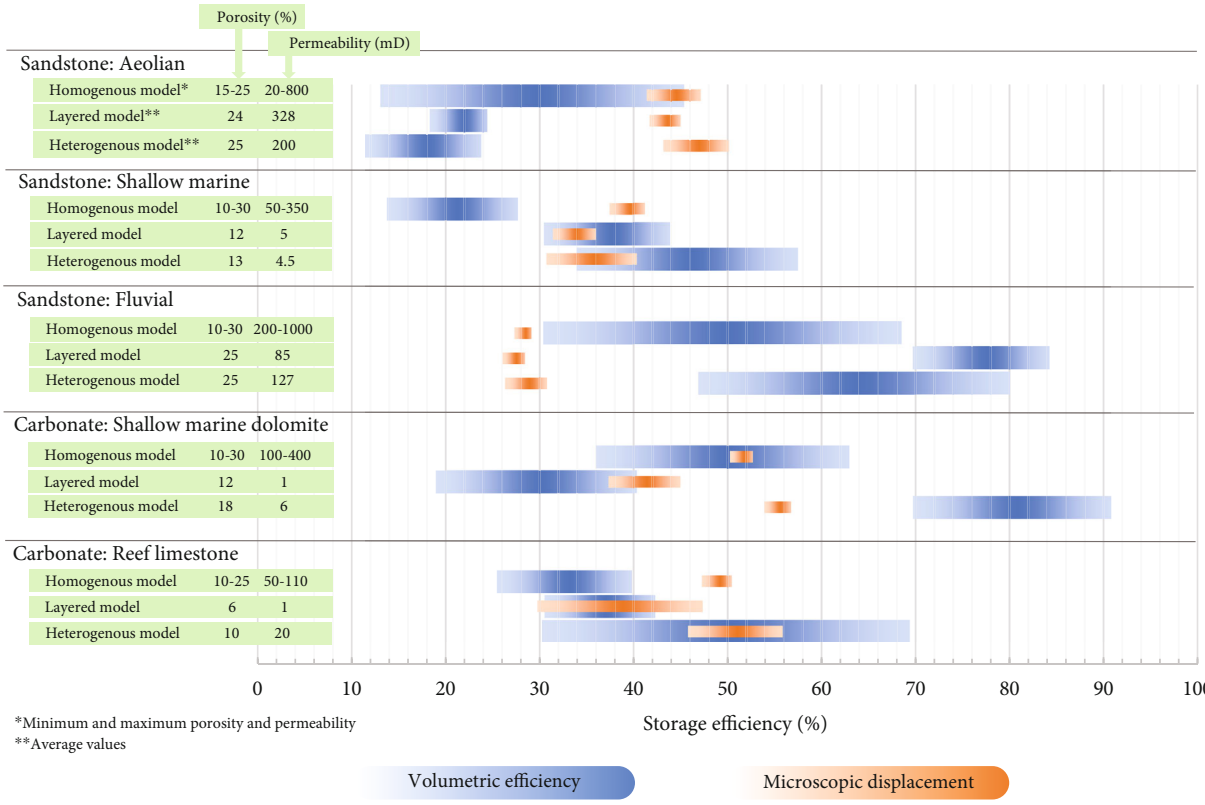

Figure 3: Impact of heterogeneity on probability distribution of the efficiencies at 30 years of CO_2 injection. The values of the homogeneous models were obtained from Haeri et al. [29].

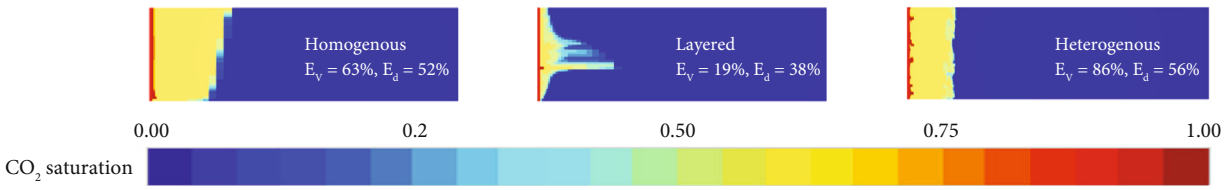

Figure 4: Variations of CO_2 plume shape and storage efficiencies for a modeling case of carbonate/shallow marine dolomite at 30 years of injection.

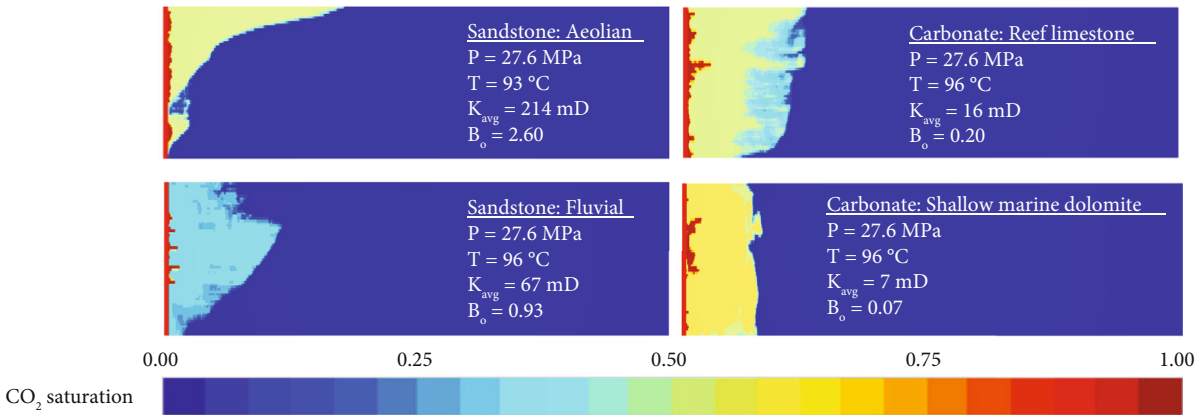

Figure 5: Variation of plume shape at 30 years of CO_2 injection in select depositional environments and lithologies using heterogeneous reservoir models. P: pressure; T: temperature; K_{avg}, average permeability; B_o: the dimensionless number.

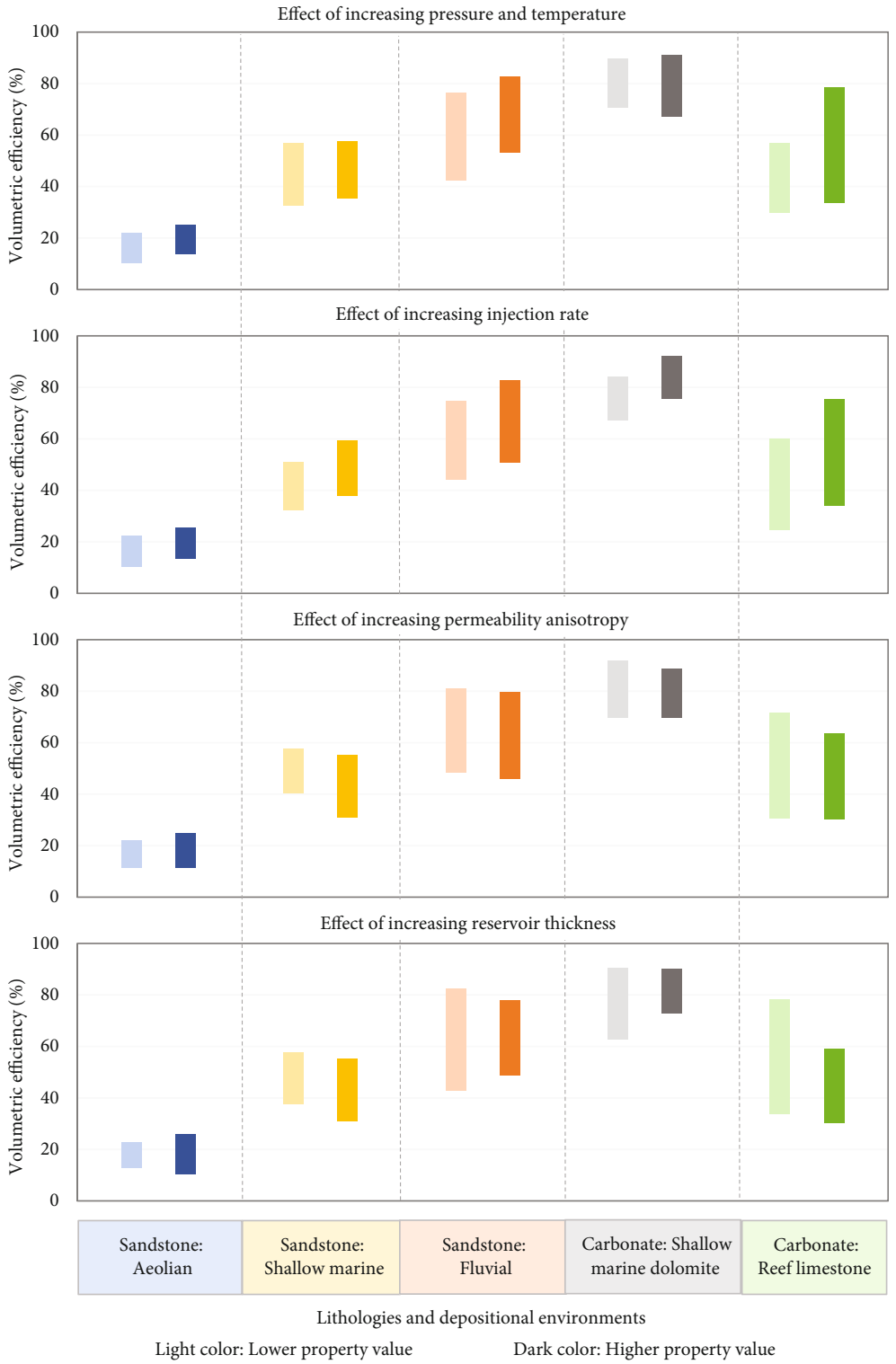

Figure 6: Impact of various pertinent parameters on volumetric efficiency at 30 years of CO_2 injection in select depositional environments and lithologies.

where $\Delta\rho$, σ, and θ are the density difference of two fluids, interfacial tension, and contact angle between supercritical CO_2 and brine at storage conditions, respectively, g is the gravitational constant, and k_V is the average vertical permeability of the formation.

Figure 5 illustrates distinctly different plume shapes for selected cases at 30 years of injection resulting from an interplay between those forces. These simulation cases use an injection rate of 800 tons/d and permeability anisotropy of 0.1. The B_o number together with the average permeability,

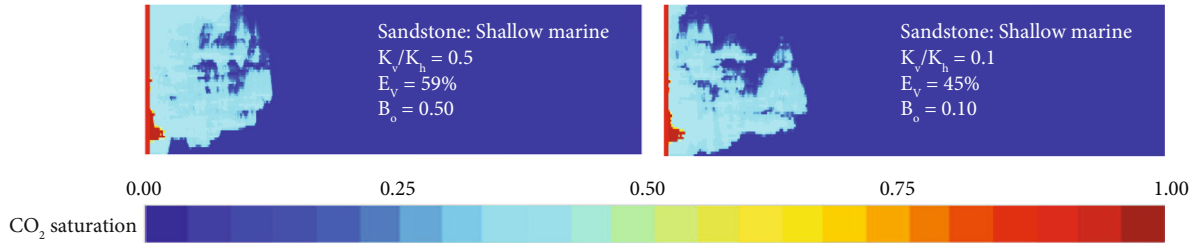

Figure 7: Effect of permeability anisotropy on volumetric efficiency and the B_o number in the sandstone shallow marine using pressure = 27.6 MPa, temperature = 88°C, injection rate = 800 t/d, and K_{avg} = 8 mD at 30 years of CO_2 injection.

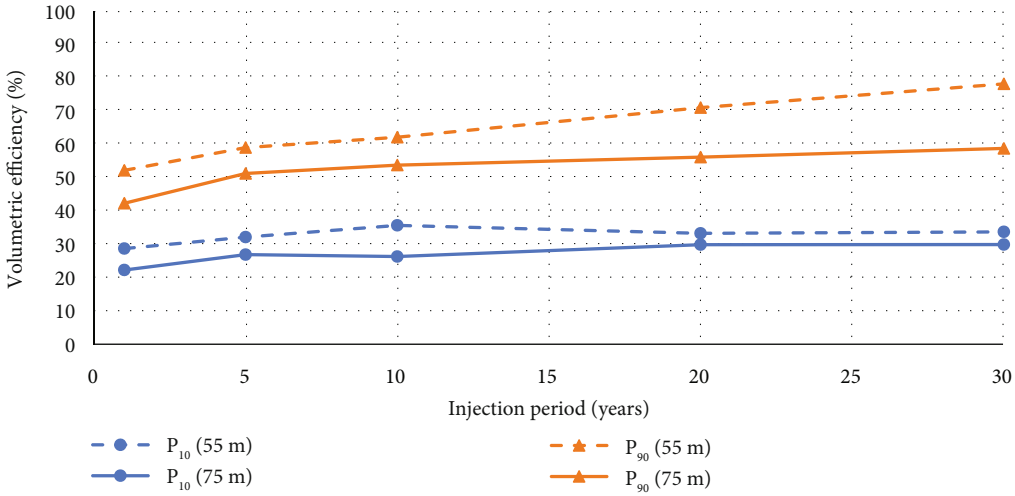

Figure 8: Impact of reservoir thickness on volumetric efficiency ranges during the 30 years of CO_2 injection in carbonate reef limestone.

pressure, and temperature conditions is depicted in Figure 5. To calculate the B_o number, the density difference between CO_2 and brine at storage conditions and permeability are averaged over the grid cells within the plume area. The average values of 27 mN/m [70–72] and average 22° [73, 74] were used for the interfacial tension and contact angle, respectively. As a general trend, the larger the B_o number, the more tendency of CO_2 to move upward reflecting the dominance of buoyancy force. In the case of the sandstone/aeolian formation ($B_o = 2.6$), the high permeability facilitates migration of CO_2 upward under the influence of density difference and its accumulation at the boundary with the seal acting as a structural trapping. On the other hand, the B_o numbers smaller than 1 indicate the dominance of capillarity resulting in retarded vertical movement and more capillary trapping in horizontal direction, as seen in Figure 4. Consequently, the B_o number serves as a criterion to determine the dominant force for flow that correlates with the resultant plume shape (Figure 4).

Both E_V and E_d are impacted by variation in the parameters listed in Table 3. However, E_V was influenced the most. Figure 6 illustrates the change in the probability distribution of E_V (P_{10}-P_{90} range) with variation of the modeling parameters, including pressure and temperature (associated with depth), permeability anisotropy, injection rate, and reservoir thickness in different depositional environments. The light and dark bars of each color correspond to minimum and maximum values of a certain parameter, respectively. Raising the pressure and temperature (i.e., going deeper in the formation) consistently shifts the efficiency distribution range upward, showing an increase in the volumetric efficiencies (Figure 6, the first plot from the top). The deep formations typically are more favorable for CO_2 storage as higher temperature associated with viscosity reduction makes the CO_2 more mobile [60]. Gorecki et al. [23] demonstrated that with increase of temperature, there is a small increase in the microscopic efficiency and a small decrease in volumetric efficiency. The impact of temperature is not studied independently in this work. However, pressure is shown to be the leading factor compared to temperature, resulting in a consistent increase in the volumetric efficiency ranges. The impact of injection rate (Figure 6, second plot from the top) is similar to pressure and temperature influence. Using a high injection rate, a larger CO_2 mass enters the reservoir for the same injection time compared to cases with a low injection rate. Consequently, capillary entry pressure is likely overcome, leading to diminishing capillary trapping and accessing more pore volume and thus higher volumetric efficiency.

The influence of permeability anisotropy is the opposite (Figure 6, third plot from the top). Increasing the permeability anisotropy (changing K_v/K_h from 0.5 to 0.1) shifts the

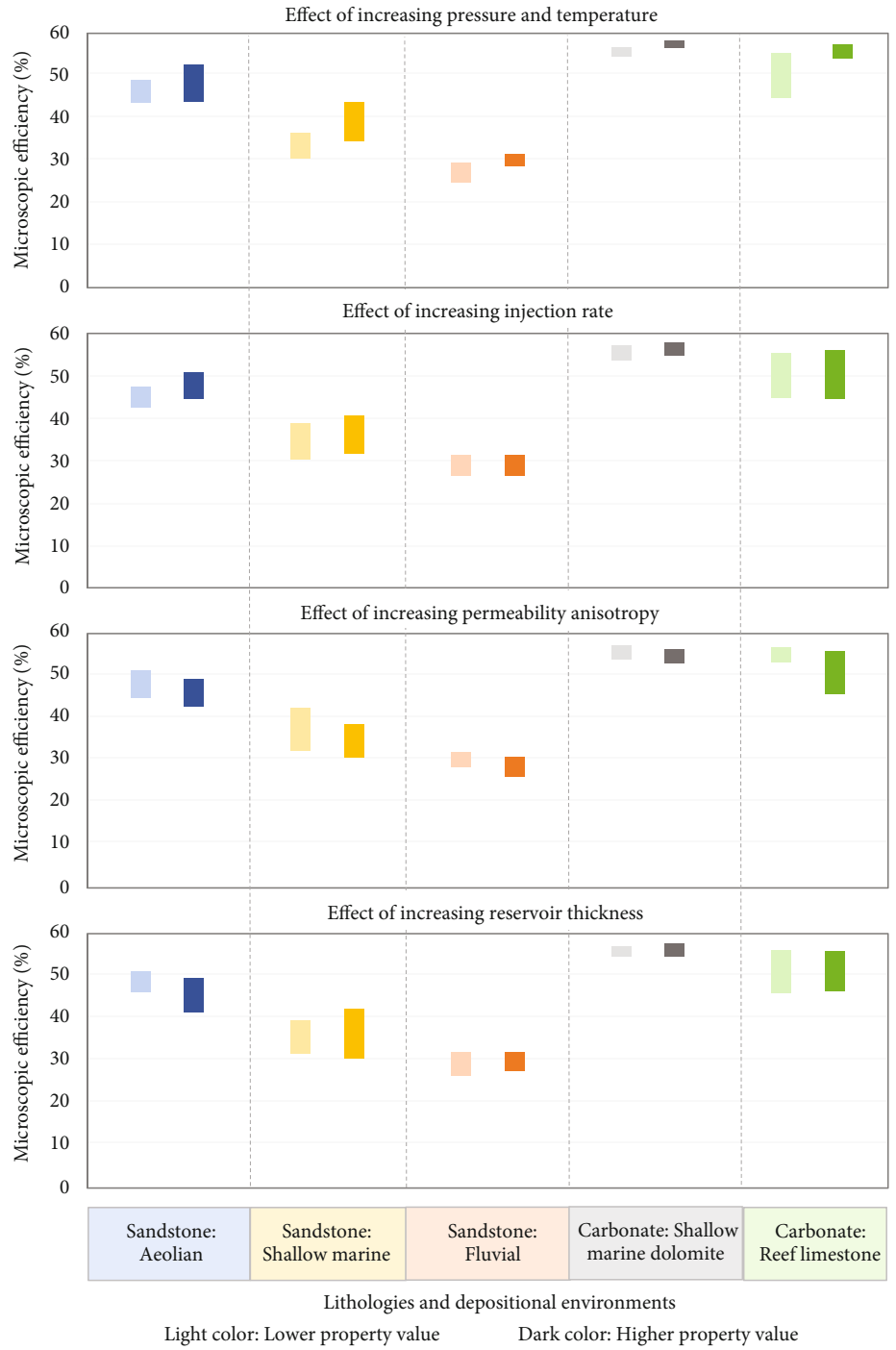

FIGURE 9: Impact of various pertinent parameters on microscopic efficiency at 30 years of CO_2 injection in select depositional environments and lithologies.

volumetric efficiency ranges downward (i.e., reduction in volumetric efficiency). With more contrast permeability anisotropy, CO_2 moves predominantly in the lateral direction that leads to a decrease in volumetric efficiency. In other words, the mechanism of CO_2 fluid flow is shifted from buoyancy-driven to permeability-controlled by the predominant flow in the horizontal direction.

An exception is the sandstone/aeolian case, in which the average permeability is high enough to compensate the lateral flow advantage with transverse buoyancy flow, leading to volumetric efficiency being insensitive to the variation of permeability anisotropy. To illustrate the influence of permeability anisotropy, Figure 7 depicts the plume shapes for the sandstone/shallow marine case with a relatively more drastic E_V reduction under the influence of an increase in permeability anisotropy. The reduction of the B_o number correlates with more extensive plume propagation in the lateral direction under the dominance of capillary forces, when

Table 4: Calculated dynamic storage efficiencies for studied lithologies and depositional environments.

Lithology: depositional environment	Injection years	Volumetric displacement (E_V)			Microscopic displacement (E_d)			Product* of (E_V) × (E_d)		
		P_{10}	P_{50}	P_{90}	P_{10}	P_{50}	P_{90}	P_{10}	P_{50}	P_{90}
Sandstone: aeolian	1	14.6	24.2	34.4	36.1	39.6	44.7	5.8	9.3	14.0
	5	12.2	16.6	24.0	38.7	43.1	47.8	5.2	7.4	10.5
	10	12.0	15.8	22.7	40.2	45.0	49.2	5.2	7.4	10.3
	20	11.9	16.6	24.5	42.2	46.3	49.7	5.4	8.0	11.4
	30	11.4	16.0	23.9	43.2	47.3	50.2	5.3	7.8	11.2
Sandstone: shallow marine	1	17.2	25.2	35.5	28.9	32.4	35.5	5.4	8.1	11.7
	5	23.9	30.2	38.7	30.3	33.6	37.0	7.9	10.3	13.2
	10	26.4	35.5	46.4	29.3	33.3	37.1	8.5	11.8	15.8
	20	31.8	43.3	54.0	30.5	34.0	37.7	10.6	14.4	18.7
	30	33.9	44.6	57.4	30.7	35.2	40.3	11.7	16.0	21.0
Sandstone: fluvial	1	40.2	51.4	62.4	22.2	24.7	27.2	9.7	12.6	15.7
	5	47.0	62.2	75.8	24.2	26.7	29.0	12.2	16.5	20.6
	10	49.2	65.2	78.5	24.8	27.6	29.8	13.2	17.7	21.8
	20	48.7	66.0	79.9	26.0	28.6	30.5	13.6	18.5	22.7
	30	46.8	65.1	80.0	26.3	29.1	30.8	13.2	18.6	23.1
Carbonate: shallow marine dolomite	1	37.8	49.1	66.4	49.4	51.1	52.6	19.3	26.8	33.9
	5	50.1	67.7	81.2	51.4	53.5	55.5	26.6	36.1	43.5
	10	58.8	76.2	86.5	52.4	54.5	56.1	31.8	40.7	47.2
	20	69.0	80.5	88.9	53.4	55.1	56.5	37.9	44.5	49.1
	30	69.6	81.6	90.8	53.8	55.3	56.7	38.4	45.6	50.3
Carbonate: reef limestone	1	25.0	35.0	49.9	30.2	34.9	43.2	8.7	13.2	18.8
	5	28.4	41.6	55.2	35.3	44.2	52.1	11.8	17.8	25.3
	10	31.3	41.9	58.7	39.2	48.4	54.7	13.9	20.7	28.4
	20	32.0	46.0	65.6	43.1	52.4	55.6	15.4	23.8	33.2
	30	30.3	47.6	69.3	45.8	53.3	55.8	15.0	25.0	35.4

*Equation (3) assuming E_A, E_h, and E_ϕ to be equal to 1.0.

$K_v/K_h = 0.1$. The capillary trapping makes the propagation front uneven with multiple areas of elevated CO_2 saturations.

Increasing the reservoir thickness leads to decreasing both P_{10} and P_{90} values for sandstone/shallow marine and carbonate/reef limestone. For the remaining lithology/deposition, the changes of P_{10} and P_{90} with thickness increase occur in different directions (Figure 6, bottom plot). That means that thickness may be strongly coupled with other reservoir parameters and implemented heterogeneity. It should be noted that in most cases, the trends of the parameter impact on P_{10} and P_{90} values remain preserved over the course of 30 years of injection.

As an example, Figure 8 displays dynamic changes of the efficiency values with time for carbonate/reef limestone. The P_{10} and P_{90} values of the higher thickness remain under corresponding storage efficiencies of the lower thickness over the course of 30 years of injection.

The effect of the modeling parameters and injection rate on E_d is less pronounced compared to E_V. Figure 9 shows the microscopic efficiency terms affected by those parameters and the rate. There is a general increasing trend in efficiencies with increasing depth (higher pressure and temperature). Similar trend is found for the volumetric efficiency that agrees with the previous work using the homogeneous reservoirs [23, 29]. The permeability anisotropy contrast (changing K_v/K_h from 0.5 to 0.1) undermines the ability of CO_2 to displace brine and, thus, decreases the microscopic efficiency (similar trend with the volumetric efficiency) in all the selected lithologies and depositional environments. This finding is different than what was found in the previous work [29] that showed little sensitivity of the efficiency terms on anisotropy after a few years of injection using homogeneous reservoir models. There is a general trend of increase of the P_{90} value for E_d with an increase of injection rate while effect of thickness shows no certain trend across all cases. That implies that for a reservoir with dominance of one lithology and depositional environment, the thickness of a formation plays little role in microscopic efficiency.

Table 4 collects dynamic E_V and E_d efficiency terms and their product calculated using P_{10}, P_{50}, and P_{90} values for select time points: 1, 5, 10, 20, and 30 years. It is noticeable that efficiencies are time-dependent. After 1 year of injection, the P_{10}, P_{50}, and P_{90} values are the lowest, and then, they increase toward 5 years and get relatively flat after 10

years. During the initial stage of injection, a CO_2 plume in a target formation is not fully developed and E_V and E_d values are low. The exception belongs to E_V values of the sandstone/aeolian reservoir having high absolute permeability and allowing quick propagation of the plume. The data shown in Table 4 are transferred to the CO_2-SCREEN tool [3], and updated values are available in the online version of the tool.

In should be noted that since the efficiency terms are estimated up to 30 years of injection, reactive transport of CO_2 in the formations and the effects of geochemical reactions were not included. Although it is known that CO_2 can significantly impact pore structure, especially in carbonate reservoirs [41, 75], the data show that mineral dissolution is most likely to develop during hundreds of years (except carbonates) [76]. Similarly, since postinjection periods and possible imbibition of the displaced fluid were not accounted for, the relative permeability hysteresis effects were not included into the simulations. The estimated heterogeneous efficiency terms are designed to be applied for formations with dominant lithologies and depositional environments listed in Table 1. For a target reservoir with large variability in depositional environment within stratigraphic layering, those factors should be applied with caution. Distinct structural features like dome, anticline, and incline were not considered in this work. It should be kept in mind that the reported efficiency factors can be influenced by such structural traps and acting gravitational forces. The 2D approximation used to create the reservoir models implies that the CO_2 plume propagates uniformly from a wellbore. However, geospatial property correlation may vary in the azimuthal directions that together with possible presence of sealing faults deviate CO_2 plume expansion from its symmetrical shape. Consequently, the uncertainty in efficiency terms due to an asymmetric plume shape will increase with injection time. For our next effort, we consider studying CO_2 injection using 3D heterogeneous reservoirs and developing a methodology of efficiency terms estimation for multiple well injection scenarios.

4. Conclusions

The results of this work indicate that there is a strong effect of the reservoir parameters and injection rate on the volumetric efficiency, while microscopic efficiency is less influenced as it is evident by narrow ranges of P_{10}-P_{90} values for E_d compared to the corresponding ranges for E_V. The increase of pressure and temperature and injection rates results in a general trend of increasing efficiencies. Increasing permeability anisotropy decreases both efficiency terms contrary to prior work utilizing homogeneous reservoir models that showed little dependency. The data suggest that there is no clear trend in the efficiency changes because of using homogeneous, layered, and heterogeneous reservoir models. Layered models providing laterally homogeneous petrophysical properties cannot be considered as transition between the homogeneous and heterogeneous models in respect of storage efficiency change.

There are no consistent trends in P_{10}-P_{90} ranges comparing homogeneous and heterogeneous model results. The volumetric and microscopic efficiencies are sensitive to injection time. There is a trend of increasing efficiencies with time indicating better utilization of reservoir volumes.

The heterogeneous reservoir models using high porosity and permeability had the lowest volumetric efficiency. That was attributed to dominance of buoyancy forces leading to poor utilization of reservoir volume by the plume. For other heterogeneous reservoirs, the higher contribution of capillary forces results in better E_V values (expressed through P_{10} and P_{90} values). It is shown that tighter reservoirs with low permeability and porosity demonstrate higher E_V and E_d, implying more efficient volume and pore network utilization. In other words, higher efficiency factors do not mean that more CO_2 can be placed in a formation, rather that the available volume and pore space will be more fully filled. A low porosity reservoir with a high-efficiency factor might hold less CO_2 than a high porosity reservoir with a low-efficiency factor.

Data Availability

The data used to support the findings of this study are available from the corresponding author upon request.

Disclosure

This research was supported in part by an appointment to the National Energy Technology Laboratory Research Participation Program, sponsored by the U.S. Department of Energy. Neither the United States Government nor any agency thereof, nor any of their employees, nor the support contractor, nor any of their employees makes any warranty, expressed or implied, or assumes any legal liability or responsibility for the accuracy, completeness, or usefulness of any information, apparatus, product, or process disclosed, or represents that its use would not infringe privately owned rights. Reference herein to any specific commercial product, process, or service by trade name, trademark, manufacturer, or otherwise does not necessarily constitute or imply its endorsement, recommendation, or favoring by the United States Government or any agency thereof. The views and opinions of authors expressed herein do not necessarily state or reflect those of the United States Government or any agency thereof.

Conflicts of Interest

The authors declare that they have no conflicts of interests.

Acknowledgments

This work was performed in support of the U.S. Department of Energy's Fossil Energy Crosscutting Technology Research Program. The research was executed through the NETL Research and Innovation Center's Carbon Storage Field Work Proposal. This project was funded by the U.S. Department of Energy, National Energy Technology Laboratory, in part, through a site support contract.

Supplementary Materials

Supplementary Material includes graphics showing an approach to determine the accessible rock volume, porosity and intrinsic permeability logs and their average value distributions for reservoir models of select lithologies and depositional environments, and images of the samples with geological descriptions. *(Supplementary Materials)*

References

[1] S. Frailey, G. Koperna, and O. Tucker, "The CO_2 Storage Resources Management System (SRMS): toward a common approach to classifying, categorizing, and quantifying storage resources," in *The 14th International Conference on Greenhouse Gas Control Technology*, Melborne, Australia, 2018.

[2] S. Sanguinito, H. Singh, E. M. Myshakin et al., "Methodology for estimating the prospective CO_2 storage resource of residual oil zones at the national and regional scale," *International Journal of Greenhouse Gas Control*, vol. 96, article 103006, 2020.

[3] S. Sanguinito, A. L. Goodman, and F. Haeri, *CO_2 Storage prospeCtive Resource Estimation Excel aNalysis (CO2-SCREEN), User's Manual*, NETL Technical Report Series, U.S. Department of Energy, National Energy Technology Laboratory, Pittsburgh, PA, USA, 2020, 2023, https://edx.netl.doe.gov/dataset/co2-screen.

[4] J. S. Levine, I. Fukai, D. J. Soeder et al., "U.S. DOE NETL methodology for estimating the prospective CO_2 storage resource of shales at the national and regional scale," *International Journal of Greenhouse Gas Control*, vol. 51, pp. 81–94, 2016.

[5] A. L. Goodman, G. Bromhal, B. Strazisar et al., *Comparison of Publicly Available Methods for Development of Geologic Storage Estimates for Carbon Dioxide in Saline Formations*, NETL Technical Report Series, U.S. Department of Energy, National Energy Technology Laboratory, Morgantown, WV, USA, 2013.

[6] US-DOE-NETL, *Carbon Sequestration Atlas of the United State and Canada*, U.S. Deparment of Energy, National Energy Technology Laboratory, Office of Fossil Energy, Second edition edition, 2008.

[7] US-DOE-NETL, *Carbon Sequestration Atlas of the United State and Canada*, U.S. Department of Energy, National Energy Technology Laboratory, Office of Fossil Energy, Third edition edition, 2010.

[8] US-DOE-NETL and K. Clay, *Carbon Utilization and Storage Atlas*, U.S. Deparment of Energy, National Energy Technology Laboratory, Office of Fossil Energy, Fourth Edition edition, 2012.

[9] A. L. Goodman, A. Hakala, G. Bromhal et al., "U.S. DOE methodology for the development of geologic storage potential for carbon dioxide at the national and regional scale," *International Journal of Greenhouse Gas Control*, vol. 5, no. 4, pp. 952–965, 2011.

[10] US-DOE-NETL, *Regional Carbon Sequestration Partnerships Initiative*, 2022, 2023, https://netl.doe.gov/carbon-management/carbon-storage/RCSP.

[11] A. L. Goodman, S. Sanguinito, and J. S. Levine, "Prospective CO_2 saline resource estimation methodology: refinement of existing US-DOE-NETL methods based on data availability," *International Journal of Greenhouse Gas Control*, vol. 54, pp. 242–249, 2016.

[12] S. Bachu, "Review of CO_2 storage efficiency in deep saline aquifers," *International Journal of Greenhouse Gas Control*, vol. 40, pp. 188–202, 2015.

[13] Q. Shao, M. Boon, A. Youssef, K. Kurtev, S. M. Benson, and S. K. Matthai, "Modelling CO_2 plume spreading in highly heterogeneous rocks with anisotropic, rate-dependent saturation functions: a field-data based numeric simulation study of Otway," *International Journal of Greenhouse Gas Control*, vol. 119, article 103699, 2022.

[14] Z. Rasheed, A. Reza, R. Gholami, M. Rabiei, A. Ismail, and V. Rasouli, "A numerical study to assess the effect of heterogeneity on CO_2 storage potential of saline aquifers," *Energy Geoscience*, vol. 1, no. 1-2, pp. 20–27, 2020.

[15] R. S. Jayne, H. Wu, and R. M. Pollyea, "Geologic CO_2 sequestration and permeability uncertainty in a highly heterogeneous reservoir," *International Journal of Greenhouse Gas Control*, vol. 83, pp. 128–139, 2019.

[16] M. Abbaszadeh and S. M. Shariatipour, "Investigating the impact of reservoir properties and injection parameters on carbon dioxide dissolution in saline aquifers," *Fluids*, vol. 3, no. 4, p. 76, 2018.

[17] B. Issautier, S. Viseur, P. Audigane, C. Chiaberge, and Y. LeNindre, "A new approach for evaluating the impact of fluvial type heterogeneity in CO_2 storage reservoir modeling," *Comptes Rendus Geoscience*, vol. 348, no. 7, pp. 531–539, 2016.

[18] E. Saadatpoor, S. L. Bryant, and K. Sepehrnoori, "New trapping mechanism in carbon sequestration," *Transport in Porous Media*, vol. 82, no. 1, pp. 3–17, 2010.

[19] S. E. Greenberg, R. Bauer, R. Will et al., "Geologic carbon storage at a one million tonne demonstration project: lessons learned from the Illinois Basin - Decatur Project," *Energy Procedia*, vol. 114, pp. 5529–5539, 2017.

[20] S. J. Jackson, S. Agada, C. A. Reynolds, and S. Krevor, "Characterizing drainage multiphase flow in heterogeneous sandstones," *Water Resources Research*, vol. 54, no. 4, pp. 3139–3161, 2018.

[21] C. Harris, S. J. Jackson, G. P. Benham, S. Krevor, and A. H. Muggeridge, "The impact of heterogeneity on the capillary trapping of CO_2 in the Captain Sandstone," *International Journal of Greenhouse Gas Control*, vol. 112, article 103511, 2021.

[22] T. Ajayi, J. S. Gomes, and A. Bera, "A review of CO_2 storage in geological formations emphasizing modeling, monitoring and capacity estimation approaches," *Petroleum Science*, vol. 16, no. 5, pp. 1028–1063, 2019.

[23] C. D. Gorecki, J. A. Sorensen, J. M. Bremer et al., "Development of storage coefficients for determining the effective CO_2 storage resource in deep saline formations," in *Paper presented at the SPE International Conference on CO2 Capture, Storage, and Utilization*, San Diego, California, USA, 2009.

[24] P. Okwen, F. Yang, and S. Frailey, "Effect of geologic depositional environment on CO_2 storage efficiency," *Energy Procedia*, vol. 63, pp. 5247–5257, 2014.

[25] J. Craig, C. D. Gorecki, S. C. Ayash, G. Liu, and J. R. Braunberger, "A comparison of volumetric and dynamic storage efficiency in deep saline reservoirs: an overview of IEAGHG study IEA/CON/13/208," *Energy Procedia*, vol. 63, pp. 5185–5191, 2014.

[26] L. J. Pekot, S. Ayash, J. Ge, T. Jiang, L. Jacobson, and C. Gorecki, "CO_2 storage efficiency in deep saline formations – stage 2," in *The 14th International Conference on Greenhouse Gas Control Technology*, Melborne, Australia, 2019.

[27] M. A. A. Al-qaness, A. A. Ewees, H. V. Thanh, A. M. Al-Rassas, A. Dahou, and M. A. Elaziz, "Predicting CO_2 trapping in deep saline aquifers using optimized long short-term memory," *Environmental Science and Pollution Research*, vol. 30, no. 12, pp. 33780–33794, 2023.

[28] H. Vo Thanh, Y. Sugai, and K. Sasaki, "Application of artificial neural network for predicting the performance of CO_2 enhanced oil recovery and storage in residual oil zones," *Scientific Reports*, vol. 10, no. 1, article 18204, 2020.

[29] F. Haeri, E. M. Myshakin, S. Sanguinito et al., "Simulated CO_2 storage efficiency factors for saline formations of various lithologies and depositional environments using new experimental relative permeability data," *International Journal of Greenhouse Gas Control*, vol. 119, p. 103720, 2022.

[30] Y. Jung, G. S. H. Pau, S. Finsterle, and C. Doughty, *TOUGH3 User's Guide, Version 1.0*, Energy Geosciences Division, Lawrence Berkeley National Laboratory, 2018.

[31] D. Crandall, J. Moore, S. Brown, and S. King, *NETL-CO_2BRA Relative Permeability Database*, U.S. Deparment of Energy, National Energy Technology Laboratory, 2019.

[32] NETL, Battelle, *Final Report CO_2 Injection Test in the Cambrian-aAge Mt. Simon Formation Duke Energy East Bend Generating Station, Boone County, Kentucky*, DOE-NETL Cooperative Agreement DE-FC26-05NT42589, 2021.

[33] Q. Zhou, X. Yang, R. Zhang et al., "Dynamic processes of CO_2 storage in the field: 1. Multiscale and multipath channeling of CO_2 flow in the hierarchical fluvial reservoir at Cranfield, Mississippi," *Water Resources Research*, vol. 56, article e2019EF001360, 2020.

[34] W. A. Peck, N. A. Azzolina, D. V. Nakles et al., *North Dakota Integrated Carbon Storage Complex Feasibility Study*, University of North Dakota Energy & Environmental Research Center, 2020, Final report.

[35] R. O. Willis, "Upper Mississippian-Lower Pennsylvanian stratigraphy of Central Montana and Williston basin," *American Association of Petroleum Geologists Bulletin*, vol. 43, no. 8, pp. 1940–1966, 1959.

[36] NETL, "Big Sky Carbon Sequestration Partnership, Danielson 33-17 Well Core Data," 2014, 2023, https://edx.netl.doe.gov/dataset/danielson-33-17-core-data.

[37] M. Kelley, A. Haagsma, P. Champagne et al., *Integrated Pre-Feasibility Assessment for a Northern Michigan Basin Carbon-SAFE CO_2 Storage Complex*, Battelle, Richland, WA, USA, 2018.

[38] N. Moodie, F. Pan, W. Jia, and B. McPherson, "Impacts of relative permeability formulation on forecasts of CO_2 phase behavior, phase distribution, and trapping mechanisms in a geologic carbon storage reservoir," *Greenhouse Gases: Science and Technology*, vol. 7, no. 5, pp. 958–962, 2017.

[39] M. Oostrom, M. D. White, S. L. Porse, S. C. M. Krevor, and S. A. Mathias, "Comparison of relative permeability-saturation-capillary pressure models for simulation of reservoir CO_2 injection," *International Journal of Greenhouse Gas Control*, vol. 45, pp. 70–85, 2016.

[40] J. Moore, P. Holcomb, D. Crandall et al., "Rapid determination of supercritical CO_2 and brine relative permeability using an unsteady-state flow method," *Advances in Water Resources*, vol. 153, article 103953, 2021.

[41] S. Benson, F. Hingerl, L. Zuo et al., *Relative Permeability for Multi-Phase Ow in CO2 Storage Reservoirs. Part II: Resolving Fundamental Issues and Filling Data Gaps*, Global CCS Institute Special Report, 2015.

[42] X. Chen, A. Kianinejad, and D. A. DiCarlo, "An experimental study of CO_2-brine relative permeability in sandstone," in *Proceedings, SPE Symposium on Improved Oil Recovery*, Tulsa, Oklahoma, USA, 2014.

[43] X. Chen and D. A. DiCarlo, "A new unsteady-state method of determining two-phase relative permeability illustrated by CO_2-brine primary drainage in Berea sandstone," *Advances in Water Resources*, vol. 96, pp. 251–265, 2016.

[44] X. Chen, A. Kianinejad, and D. A. DiCarlo, "Direct measurement of relative permeability in rocks from unsteady-state saturation profiles," *Advances in Water Resources*, vol. 94, pp. 1–10, 2016.

[45] G. S. Jeong, S. Ki, D. S. Lee, and I. Jang, "Effect of the flow rate on the relative permeability curve in the CO_2 and brine system for CO_2 sequestration," *Sustainability*, vol. 13, no. 3, p. 1543, 2021.

[46] NETL, "Kevin Dome static model development final report," 2018, https://edx.netl.doe.gov/dataset/kevin-dome-geologic-model, 2023.

[47] WinGSLib, "Geostatistical software and services," http://www.statios.com/WinGslib/index.html, 2023.

[48] R. H. Hugman, P. S. Springer, E. H. Vidas, and R. Long, "Lower-48 oil and gas resource characterization with the GASIS database," 2016, https://edx.netl.doe.gov/dataset/lower-48-oil-and-gas-resource-characterization-with-the-gasis-database, 2023.

[49] A. Al-Menhali, B. Niu, and S. Krevor, "Capillarity and wetting of carbon dioxide and brine during drainage in Berea sandstone at reservoir conditions," *Water Resources Research*, vol. 51, no. 10, pp. 7895–7914, 2015.

[50] R. Pini and S. M. Benson, "Capillary pressure heterogeneity and hysteresis for the supercritical CO_2/water system in a sandstone," *Advances in Water Resources*, vol. 108, pp. 277–292, 2017.

[51] S. Wang and T. T. Tokunaga, "Capillary pressure–saturation relations for supercritical CO_2 and brine in limestone/dolomite sands: implications for geologic carbon sequestration in carbonate reservoirs," *Environmental Science & Technology*, vol. 9, no. 12, pp. 7208–7217, 2015.

[52] J. B. Clavaud, A. Maineult, M. Zamora, P. Rasolofosaon, and C. Schlitter, "Permeability anisotropy and its relations with porous medium structure," *Journal of Geophysical Research*, vol. 113, no. B1, article B01202, 2008.

[53] M. Sato, K. Panaghi, N. Takada, and M. Takeda, "Effect of bedding planes on the permeability and diffusivity anisotropies of Berea sandstone," *Transport in Porous Media*, vol. 127, no. 3, pp. 587–603, 2019.

[54] K. Pruess and ECO2M, *A TOUGH2 Fluid Property Module for Mixtures of Water, NaCl, and CO_2, Including Super- and Subcritical Conditions, and Phase Change between Liquid and Gaseous CO_2*, Earth Sciences Division, Lawrence Berkeley National Laboratory, 2011, https://tough.lbl.gov/assets/docs/TOUGH2-ECO2M_Users_Guide.pdf, 2023.

[55] PetraSim, User Manual, "Thunderhead engineering," 2018, https://www.thunderheadeng.com/wp-content/uploads/dlm_uploads/2015/04/PetraSimManual-4.pdf, 2023.

[56] Y. Debbabi, M. D. Jackson, G. J. Hampson, and P. Salinas, "Impact of the buoyancy–viscous force balance on two-phase flow in layered porous media," *Transport in Porous Media*, vol. 124, no. 1, pp. 263–287, 2018.

[57] D. Zhou, F. J. Fayers, and F. M. Orr Jr., "Scaling of multiphase flow in simple heterogeneous porous media," in *Paper*

presented at the SPE/DOE Improved Oil Recovery Symposium, p. 12, Tulsa, Oklahoma, 1994.

[58] R. Gharbi, E. Peters, and A. Elkamel, "Scaling miscible fluid displacements in porous media," *Energy & Fuels*, vol. 12, no. 4, pp. 801–811, 1998.

[59] Y. Cinar, K. Jessen, R. Berenblyum, R. Juanes, and F. M. Orr Jr., "An experimental and numerical investigation of crossflow effects in two-phase displacements," *SPE Journal*, vol. 11, no. 2, pp. 216–226, 2006.

[60] A. Kopp, H. Class, and R. Helmig, "Investigations on CO_2 storage capacity in saline aquifers: part 1. Dimensional analysis of flow processes and reservoir characteristics," *International Journal of Greenhouse Gas Control*, vol. 3, no. 3, p. 263, 2009.

[61] R. G. Larson, H. T. Davis, and L. E. Scriven, "Displacement of residual nonwetting fluid from porous media," *Chemical Engineering Science*, vol. 36, no. 1, pp. 75–85, 1981.

[62] I. Chatzis and N. R. Morrow, "Correlation of capillary number relationships for sandstone," *SPE Journal*, vol. 24, no. 5, pp. 555–562, 1984.

[63] N. R. Morrow, I. Chatzis, and J. J. Taber, "Entrapment and mobilization of residual oil in bead packs," *SPE Reservoir Engineering*, vol. 3, no. 3, pp. 927–934, 1988.

[64] L. W. Lake, *Enhanced Oil Recovery*, Prentice Hall, Englewood Cliffs, N.J, 1989.

[65] R. Hilfer and P. E. Oren, "Dimensional analysis of pore scale and field scale immiscible displacement," *Transport in Porous Media*, vol. 22, no. 1, pp. 53–72, 1996.

[66] M. Shook, D. Li, and L. Lake, "Scaling immiscible flow through permeable media by inspectional analysis," *In Situ*, vol. 16, no. 4, pp. 311–349, 1992.

[67] C. Kuo and S. M. Benson, "Analytical study of effects of flow rate, capillarity, and gravity on CO_2/brine multiphase-flow system in horizontal corefloods," *SPE Journal*, vol. 18, no. 4, pp. 708–720, 2013.

[68] L. Trevisan, A. Cihan, F. Fagerlund et al., "Investigation of mechanisms of supercritical CO_2 trapping in deep saline reservoirs using surrogate fluids at ambient laboratory conditions," *International Journal of Greenhouse Gas Control*, vol. 29, pp. 35–49, 2014.

[69] R. Ben, "Local capillary trapping in carbon sequestration: parametric study and implications for leakage assessment," *International Journal of Greenhouse Gas Control*, vol. 78, pp. 135–147, 2018.

[70] Z. Li, S. Wang, S. Li, W. Liu, B. Li, and Q. Lv, "Accurate determination of the CO_2–brine interfacial tension using graphical alternating conditional expectation," *Energy & Fuels*, vol. 28, no. 1, pp. 624–635, 2014.

[71] Y. Liu, H. Li, and R. Okuno, "Measurements and modeling of interfacial tension for CO_2/CH_4/brine systems under reservoir conditions," *Industrial and Engineering Chemistry Research*, vol. 55, no. 48, pp. 12358–12375, 2016.

[72] L. M. C. Pereira, A. Chapoy, R. Burgass, and B. Tohidi, "Interfacial tension of CO_2 + brine systems: experiments and predictive modelling," *Advances in Water Resources*, vol. 103, pp. 64–75, 2017.

[73] F. Haeri, D. Tapriyal, S. Sanguinito et al., "CO_2–brine contact angle measurements on Navajo, Nugget, Bentheimer, Bandera Brown, Berea, and Mt. Simon Sandstones," *Energy & Fuels*, vol. 34, no. 5, pp. 6085–6100, 2020.

[74] F. Haeri, D. Tapriyal, C. Matranga, D. Crandall, and A. Goodman, "Variation of CO_2-brine contact angles on natural rocks of different compositions," *Journal of Energy and Power Technology*, vol. 3, no. 4, p. 046, 2021.

[75] M. Seyyedi, H. K. Mahmud, M. Verrall et al., "Pore structure changes occur during CO_2 injection into carbonate reservoirs," *Scientific Reports*, vol. 10, no. 1, p. 3624, 2020.

[76] J. Ennis-King and L. Paterson, "Rate of dissolution due to convective mixing in the underground storage of carbon dioxide," *International Journal of Greenhouse Gas Control*, vol. I, pp. 507–510, 2003.